Catalysis Science & Technology

Nanostructured Ni-Cu Electrocatalysts for the Oxygen Evolution Reaction

Journal:	*Catalysis Science & Technology*
Manuscript ID	CY-ART-03-2020-000427.R1
Article Type:	Paper
Date Submitted by the Author:	10-Jun-2020
Complete List of Authors:	Gautam, Rajendra; University of Nevada, Reno, Department of Chemistry; Pan, Hanqing; University of Nevada, Reno, Department of Chemistry Chalyavi, Farzaneh; University of Nevada Reno, Tucker, Matthew; University of Nevada, Reno, Department of Chemistry Barile, Christopher; University of Nevada, Reno, Department of Chemistry

Nanostructured Ni-Cu Electrocatalysts for the Oxygen Evolution Reaction

Rajendra P. Gautam, Hanqing Pan, Farzaneh Chalyavi,

Matthew J. Tucker, and Christopher J. Barile*

Department of Chemistry, University of Nevada, Reno, Nevada 89557, USA

*Corresponding author: cbarile@unr.edu

Keywords: nanoclusters, oxygen evolution reaction, electrocatalysts, bimetallic

Abstract

Ni-based materials are promising electrocatalysts for the oxygen evolution reaction (OER) for water splitting in alkaline media. We report the synthesis and OER electrocatalysis of both Ni-Cu nanoparticles (20-50 nm in diameter) and Ni-Cu nanoclusters (<20 metal atoms). Analysis of mass spectral data from matrix-assisted laser desorption/ionization and electrospray ionization techniques demonstrates that discrete heterobimetallic Ni-Cu nanoclusters capped with glutathione ligands were successfully synthesized. Ni-Cu nanoclusters with a 52:48 mol % Ni:Cu metal composition display an OER onset overpotential of 50 mV and an overpotential of 150 mV at 10 mA cm^{-2}, which makes this catalyst one of the most efficient nonprecious metal OER catalysts. The durability of the nanocluster catalysts on carbon electrodes can be extended by appending them to electrodes modified with TiO_2 nanoparticles. Infrared spectroscopy results indicate that the aggregation dynamics of the glutathione ligands change during catalysis. Taken together, these results help explain the reactivity of a novel class of nanostructured Ni-Cu OER catalysts, which are underexplored alternatives to more commonly studied Ni-Fe, Ni-Co, and Ni-Mn materials.

Introduction

The production of hydrogen gas from renewable energy is at the center of hydrogen-based energy storage schemes. One method of producing hydrogen in a clean and renewable manner is from the electrolysis of water. However, the efficiency of current water electrolyzers is limited by the slow kinetics of the oxygen evolution reaction (OER).[1-2] Although there are several possible OER mechanisms, all pathways involve several proton and electron transfer steps, which give rise to large reaction barriers and necessitate the application of high overpotentials to drive the reaction at reasonable rates. Noble metal OER catalysts such as RuO_2, IrO_2, and Pt exhibit high OER activity but their scarcity and high cost make large-scale utilization impractical.[3-5] Therefore, the development of inexpensive OER catalysts from nonprecious metals that possess high activity and good durability is still an unresolved challenge.

Ni-based bimetallic systems such as Ni-Co, Ni-Mn, and Ni-Fe are commonly explored classes of nonprecious metal OER catalysts that exhibit low overpotentials and enhanced activity compared to pure Ni. For example, Antar *et al.* electrodeposited Ni-Co thin film OER catalysts with a conducting polymer.[6] Fu *et al.* synthesized a series of Ni-Co phosphides with a cage-like structure.[7] Similarly, Qiu *et al.* designed Ni-Co phosphide nanocages by tuning the molar ratio of Ni/Co atoms that led to catalysts with an overpotential of 300 mV at 10 mA cm^{-2}.[2] Cheng *et al.* reported bimetallic Ni-Fe catalysts on N-doped carbon nanotubes that significantly enhanced OER activity by forming bridged Ni-Fe bimetallic dual atom active sites for the OER.[8] Both Nai *et al.* and Zhu *et al.* reported on porous and hollow Ni-Co oxide nanostructures that demonstrated enhanced OER activity by varying the Ni-Co composition.[9-10]

Our group recently demonstrated that Ni-Cu surfaces are another promising class of bimetallic Ni catalysts.[11] To construct Ni-Cu catalysts, we electrodeposited Ni overlayers of

different thicknesses on top of Cu_2O thin films. OER catalysts with an optimal Ni:Cu_2O ratio exhibit an onset overpotential of only 150 mV. Although these catalysts display promising onset overpotentials, they do not operate at low overpotentials at high current densities because they are bulk materials incapable of supporting high reaction rates. In this manuscript, to overcome the current density issue of the electrodeposited Ni-Cu OER catalysts, we developed nanostructured Ni-Cu systems. We synthesized bimetallic Ni-Cu nanoclusters (<20 metal atoms) and nanoparticles (20-50 nm) to increase the current density for catalysis while maintaining the low OER overpotential intrinsic to Ni-Cu systems. For both the nanoparticles and the nanoclusters, the Ni to Cu ratio significantly affects the efficiency of OER electrocatalysis. The Ni-Cu nanocluster catalyst with a 52:48 Ni-Cu mol % exhibits an onset overpotential of only ~50 mV and an overpotential of only ~150 mV at an industrially-relevant rate (10 mA cm^{-2}).

Experimental Section

General Procedures. Chemicals were obtained from commercially available sources and used without further purification. Electrochemical studies were carried out using a VSP-300 Biologic potentiostat using a three-electrode system with a Pt counter electrode, a Ag/AgCl reference electrode, and a glassy carbon working electrode. All experiments were conducted at room temperature (26 ± 1) °C in 1 M NaOH at a scan rate of 10 mV/s unless otherwise noted. Most experiments were conducted in unpurified NaOH (Oakwood Chemicals, 99%) electrolytes. For some experiments, NaOH electrolytes were purified following a literature protocol.[12] The purified and unpurified electrolytes contained 2 ppb and 115 ppb of Fe, respectively, as determined by inductively coupled plasma-mass spectrometry (ICP-MS). The OER LSVs reported were IR corrected using the solution resistance value obtained from electrochemical impedance spectroscopy. All LSV experiments were at least triplicated. Onset potentials were calculated by

determining the potential at which the current density reached 10% of its maximum current density. Tafel slopes were calculated using a voltage range of 1.2-1.8 V.

Synthesis of Nanoparticles. Nanoparticles were synthesized through a procedure modified from the work of Argueta-Figueroa *et al.*[13] For the synthesis of Cu and Ni metallic and bimetallic nanoparticles, varying amounts of $CuSO_4$ and $NiSO_4•6H_2O$ were dissolved in 100 mL water. For the synthesis of pure Cu or Ni metallic nanoparticles, 1.596 g of $CuSO_4$ or 2.809 g of $NiSO_4•6H_2O$ was dissolved in 100 mL water, and the pH of the solution was adjusted to 8 with 0.1 M NaOH. For the synthesis of 59:41 mol % Ni-Cu bimetallic nanoparticles, 1.404 g of $NiSO_4•6H_2O$ and 0.798 g $CuSO_4$ was used. Similarly, for the synthesis of 46:54 mol % Ni-Cu bimetallic nanoparticles, 0.702 g of $NiSO_4•6H_2O$ and 1.197 g $CuSO_4$ was taken. Finally, for the synthesis of 71:29 mol % Ni-Cu bimetallic nanoparticles, 2.107 g of $NiSO_4•6H_2O$ and 0.040 g $CuSO_4$ was taken. The pH of the solutions were adjusted to 8 with 0.1 M NaOH and bubbled with N_2 for at least 30 minutes. Next, 0.5 mL of 0.04 M $NaBH_4$ was added quickly under vigorous stirring and stirred for 2 hours to complete the reaction. The precipitate was then collected by vacuum filtration and washed three times with distilled water and once with acetone. Finally, the obtained nanoparticles were collected and stored under isopropyl alcohol.

Synthesis of Nanoclusters. The synthesis procedure described by Gao *et al.* was used with slight modification.[14] For the synthesis of Cu and Ni metallic and bimetallic nanoclusters, varying amounts of $CuCl_2$ and $NiCl_2$ were dissolved in 25 mL water. For the synthesis of pure Cu and Ni metallic nanoclusters, 0.169 g of $CuCl_2$ and 0.163 g of $NiCl_2$ were used. For the synthesis of 43:57 mol % Ni-Cu bimetallic nanoclusters, 0.163 g of $NiCl_2$ and 0.169 g $CuCl_2$ was taken. Similarly, for the synthesis of 25:75 mol % Ni-Cu bimetallic nanoclusters, 0.163 g of $NiCl_2$ and 0.338 g $CuCl_2$ was used. For the synthesis of 52:48 mol % Ni-Cu bimetallic nanoclusters, 0.326 g of $NiCl_2$

and 0.169 g $CuCl_2$ was taken. After dissolving the salts in 25 mL water, the metal salt solution was added to 16.5 mL aqueous solution containing 0.765 g of glutathione while stirring. After the pH of the solution dropped to 2-3, 250 μL of 50 mmol NaOH was added slowly. After 10 minutes, 0.5 mL hydrazine monohydrate was added dropwise to the reaction mixture. After 3 hours of stirring, the resulting solution was stored at 5 °C overnight. The obtained nanoclusters were then centrifuged at 3300 rpm for 3-5 minutes and washed once with ethanol. The final nanoclusters were collected by centrifugation and stored in water for further use.

Experiments on Glassy Carbon Electrodes. The catalysts were loaded onto a glassy carbon electrode (0.196 cm^2 geometric area) by mixing 0.11 g of Vulcan XC-72, 0.04 g of polyvinylidene fluoride (PVDF, Kynar Flex 2751-00), and 0.01 g of catalyst in a small vial. Acetone (1.0 mL) was added to the vial and the resulting mixture was sonicated for 10 minutes. This solution (20 μL) was dropcasted onto a glassy carbon electrode and dried under a gentle stream of air for 5 minutes. Electrodes using TiO_2 nanoparticles (Anatase, ~21 nm, Sigma Aldrich) were fabricated by dropcasting a suspension of TiO_2 (10 mg/mL in acetone) onto a carbon support. After the TiO_2 has dried, Ni-Cu nanoclusters (10 mg/mL in acetone) were then dropcasted on the TiO_2/carbon substrate and dried in air.

FTIR Characterization. The FTIR spectrum of the as-synthesized 52:48 mole % Ni-Cu glutathione-nanocluster complex was collected in D_2O. The same nanocluster complex was subjected to OER catalysis in 1 M NaOH for 1 hr of chronopotentiometry at 10 mA cm^{-2} in H_2O using a glassy carbon working electrode. After catalysis, the nanoclusters were lyophilized and suspended in D_2O before FTIR was conducted. Additionally, the FTIR spectrum of the glutathione ligand in D_2O was collected to determine the signatures of free ligand in solution. All IR spectra were collected on a ThermoNicolet 6700 FTIR spectrometer, equipped with a liquid nitrogen

cooled mercury cadmium telluride (MCT) detector, at 1 cm^{-1} resolution using a homemade two-compartment CaF_2 sample cell with a 56 μm Teflon spacer. The cell was divided into two compartments to collect IR measurements of the reference and the sample under similar experimental conditions and to eliminate laser drift. An automated translation stage moved the sample cell between the reference and the sample side collecting a single beam spectrum for each side, and the final IR spectrum was processed as a ratio of the sample and reference single beam.

Other Materials Characterization. Scanning electron microscope (SEM) images were obtained using a Hitachi S-4700 II Field Emission SEM with an Energy Dispersive Spectrometer (EDX) at an acceleration voltage of 15 kV. X-ray diffraction (XRD) was performed using a Bruker D2 X-ray Diffractometer using carbon paper as a substrate (Fuel Cell Store, AvCarb EP40T). ICP-MS was conducted by Western Environmental Testing Laboratory (Sparks, NV). All Ni:Cu ratios reported in this manuscript come from ICP-MS results as opposed to the nominal ratios of the Ni and Cu salts used during synthesis. The Faradaic efficiency for O_2 evolution was determined using a SRI 8610C gas chromatograph equipped with a thermal conductivity detector and a previously described custom-built electrochemical cell.[15] Matrix-assisted laser desorption/ionization time of flight (MALDI-TOF) mass spectra were recorded on a Bruker microflex MALDI-TOF spectrometer using 2,5-dihydroxybenzoic acid as the matrix. High-resolution mass spectrometry with electrospray ionization (ESI-MS) analysis was obtained using an Agilent G6230B time-of-flight mass spectrometer. Fluorescence spectroscopy was performed with a Jobin Yvon Horiba FluoroMax-3 using an excitation wavelength of 365 nm and ethanol as a solvent.

Results and Discussion

Ni and Cu metallic and bimetallic nanoparticles were synthesized from aqueous solutions of $NiSO_4$ and $CuSO_4$ using $NaBH_4$ as a reducing agent through a modified literature procedure.[13]

SEM-EDX analysis of the bimetallic Ni-Cu nanoparticles demonstrates that the nanoparticles were successively synthesized with particle diameters ranging between 20-50 nm (Figure S1, ESI). To compare the effect of particle size on the OER electrocatalytic activity, we also synthesized metallic and bimetallic Ni-Cu nanoclusters. To form the smaller nanoclusters, glutathione is used as a stabilizing ligand that kinetically traps the particles such that they form nanoclusters containing 5-20 metal atoms. Furthermore, glutathione is a small enough ligand that it should not significantly impede electron transfer rates relative to typical OER turnover frequencies.[16] Fluorescence spectroscopy (Figure S2, ESI) indicates that the Cu nanoclusters emit visible light upon ultraviolet radiation, as has been previously shown for similar systems.[17-19] We quantified the Ni:Cu ratio of both the nanoparticles and nanoclusters using ICP-MS.

The size and composition of the Ni-Cu bimetallic nanoclusters were further characterized by MALDI-TOF MS and high resolution ESI-MS. MALDI-TOF MS of pure Cu nanoclusters synthesized using glutathione (GS) is known to yield a series of ions corresponding to bare Cu nanoclusters and Cu nanoclusters bound to the glutathione ligands.[20] The MADLI-TOF MS of pure Cu nanoclusters we synthesized also has peaks ascribable to a similar set of ions (Figure S3, Table S1, ESI). More importantly, we also conducted mass spectrometry of the bimetallic Ni-Cu nanoclusters. The most intense mass peak in the MALDI-TOF spectrum of the 52:48 mol % Ni-Cu nanoclusters occurs at a m/z of 1078.5 (Figure 1A), which within the resolution of MADLI m/z values (2-3 amu) can be assigned to either the bimetallic ion $[Cu_9Ni_3GS + Na]^+$ or the monometallic $[Cu_7GS_2 + Na]^+$ ion. The most intense peak at a similar m/z value in the MALDI-TOF spectrum of the pure Cu nanoclusters (Figure S3, ESI) suggests that the peak is due to the monometallic $[Cu_7GS_2 + Na]^+$ species. However, several other peaks in the MALDI-TOF spectrum of the 52:48 mol % Ni-Cu nanoclusters can only be assigned to ions corresponding to

bimetallic species. For example, one of the most intense peaks in the spectrum occurs at a m/z of 1343.8 (Figure 1A) and can only be ascribed to bimetallic ions such as $[Cu_6Ni_6GS_2 + H]^+$. To confirm the presence of bimetallic species, we performed high-resolution ESI-MS on the bimetallic nanoclusters (Figure 1B). The top panel in Figure 1B shows the theoretical isotopic splitting pattern for a 1:1:1 mixture of $[Cu_7Ni_5GS_2 + H]^+$, $[Cu_6Ni_6GS_2 + H]^+$, and $[Cu_5Ni_7GS_2 + H]^+$ ions. The experimental ESI-MS spectrum from 1340-1360 m/z matches well with this theoretical spectrum (bottom panel, Figure 1B), indicating that bimetallic species are indeed present in the bimetallic nanoclusters.

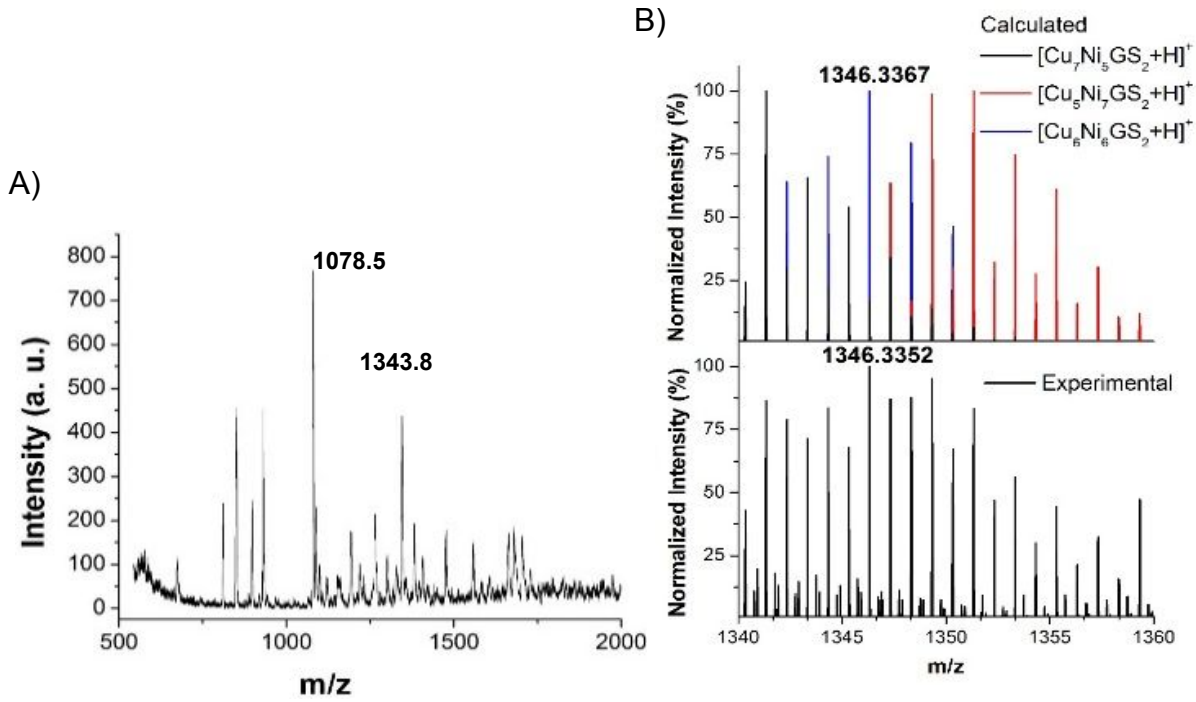

FIGURE 1. Positive-mode MALDI-TOF mass spectrum of the as-synthesized 52:48 mol % Ni-Cu nanoclusters (A). Calculated (B, top panel) isotopic pattern and experimental mass spectrum obtained from high resolution ESI mass spectrometry (B, bottom panel) of the nanoclusters.

A thorough assignment of peaks in the MALDI-TOF spectra (Figures S4-S6, ESI) for both the monometallic and bimetallic Ni-Cu nanoclusters is presented in Table S1, ESI. For all of the bimetallic nanoclusters, several additional peaks are present in the mass spectra that can only be

assigned to bimetallic clusters (bold entries in Table S1, ESI). Because these same peaks are absent from the spectra of the monometallic nanoclusters, this analysis further demonstrates that heterobimetallic clusters were formed, not just composites of individual Ni and Cu nanoclusters. MALDI-TOF MS of the Ni-Cu bimetallic nanoclusters after immersing them overnight in the 1 M NaOH electrolyte used for our OER electrocatalytic studies shows that the composition of the bimetallic nanoclusters remains the same after electrolyte immersion (Figure S7, ESI).

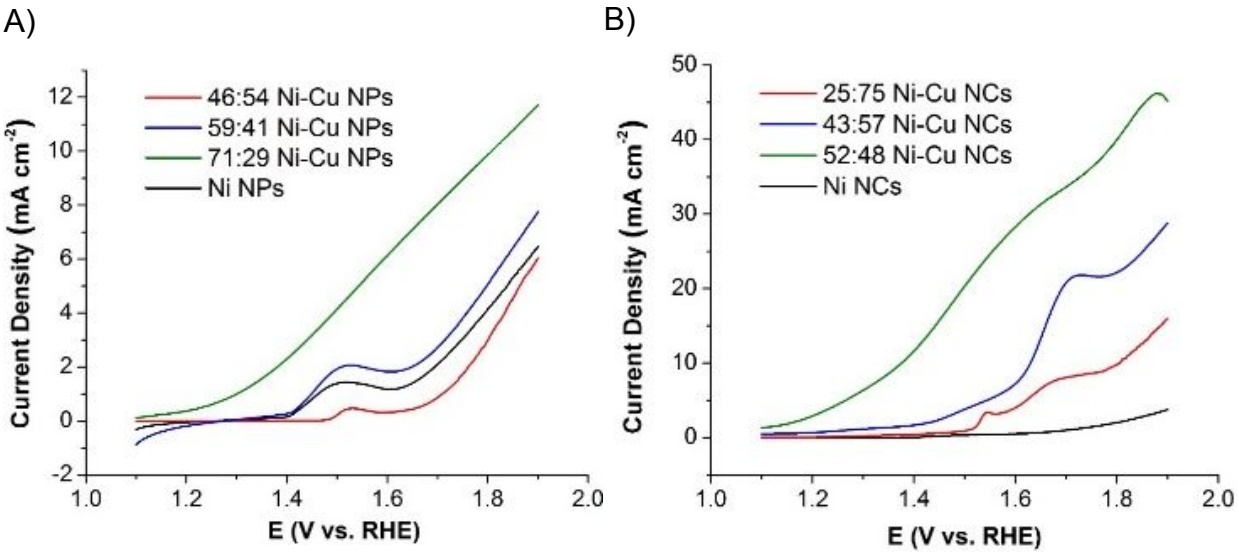

FIGURE 2. Linear sweep voltammograms at 10 mV s^{-1} of the oxygen evolution reaction in 1 M NaOH using a glassy carbon working electrode modified with a mixture of Ni-Cu bimetallic nanoparticles (NPs, A) or nanoclusters (NCs, B), Vulcan XC-72, and PVDF. Ni-Cu bimetallic NPs and NCs with various molar ratios were tested (colored lines) along with pure Ni (black lines) and pure Cu (Figure S11, ESI) NPs and NCs. Current densities are reported against the geometric electrode area.

Having synthesized an array of Cu and Ni nanostructured systems, we next assessed their ability to function as OER electrocatalysts. Catalysts were prepared on glassy carbon working electrodes, and linear sweep voltammograms (LSVs) in 1 M NaOH were conducted at a scan rate of 10 mV s^{-1}. For all catalysts, O_2 bubbles vigorously evolved from the electrode surface at voltages above 1.4 V vs. RHE. The LSVs show that the molar composition of the nanoparticles dramatically affects their OER activity (Figure 2A). The current density is highest for the 71:29 mol % Ni-Cu

bimetallic nanoparticles (green line) as compared to other compositions of bimetallic nanoparticles. For the Ni (black line), 59:41 mol % Ni-Cu (blue line), and 46:54 mol % Ni-Cu nanoparticles (red line), there is a peak at approximately 1.5 V vs. RHE. This peak has been observed previously in other Ni-based OER catalysts and is due to the electrochemical oxidation of $Ni(OH)_2$, which spontaneously forms when Ni is immersed in alkaline solutions, to NiOOH.[21] Cyclic voltammetry experiments in the appropriate voltage range demonstrate that this NiOOH can be converted back to $Ni(OH)_2$ upon reduction (Figure S8, ESI). The reason for the lack of a NiOOH peak in the LSV for the 71:29 mol % Ni-Cu is not clear. Furthermore, prominent peaks near 1.5 V are not present in the LSVs of the Ni-Cu nanoclusters. The Ni in these cases is bonded to the thiol group in the glutathione ligand, and we hypothesize that this added stability inhibits the $Ni(OH)_2$/NiOOH wave. Analagous experiments with Ni-Cu nanoclusters show that the OER current density measured is much greater than the nanoparticles due to an increase in the surface area of the small nanoclusters, which results in a greater number of active catalytic sites (Figure 2B). The results also demonstrate that like the nanoparticles, the catalytic activity of the nanoclusters depends strongly upon the molar ratio of Ni and Cu present. In particular, nanoclusters with 52:48 mol % Ni-Cu possess the highest OER current density (Figure 2B, green line). An OER LSV of the 52:48 mol % Ni-Cu nanoclusters in a purified NaOH electrolyte that contained only 2 ppb Fe is similar to the analagous LSV in an unpurified electrolyte with 115 ppb Fe (Figure S9, ESI). This finding demonstrates that possible Fe incorporation into the Ni-based catalysts from electrolyte impurities does not play a significant role in dictating catalyst activity. However, there is a small peak at approximately 1.85 V in the LSV with the unpurified electrolyte that is not present in the LSV with the purified electrolyte. These results suggest that the peak at about 1.85 V is due to the activity of a Ni-Fe species. A LSV of the 52:48 mol % Ni-Cu nanoclusters at a slower scan rate of 2 mV s^{-1} exhibits

less current density as expected, but possesses a similar onset potential as the corresponding LSV at 10 mV s^{-1} (Figure S10, ESI). Lastly, we note that the OER current densities obtained for the monometallic systems are much less than those of any of the bimetallic systems and are about 10 times less than those of the bimetallic systems with optimal compositions (Figures 2 and S11, ESI). In other words, bimetallic Ni-Cu nanoparticles and nanoclusters exhibit far superior performance than either of their pure Ni or pure Cu counterparts.

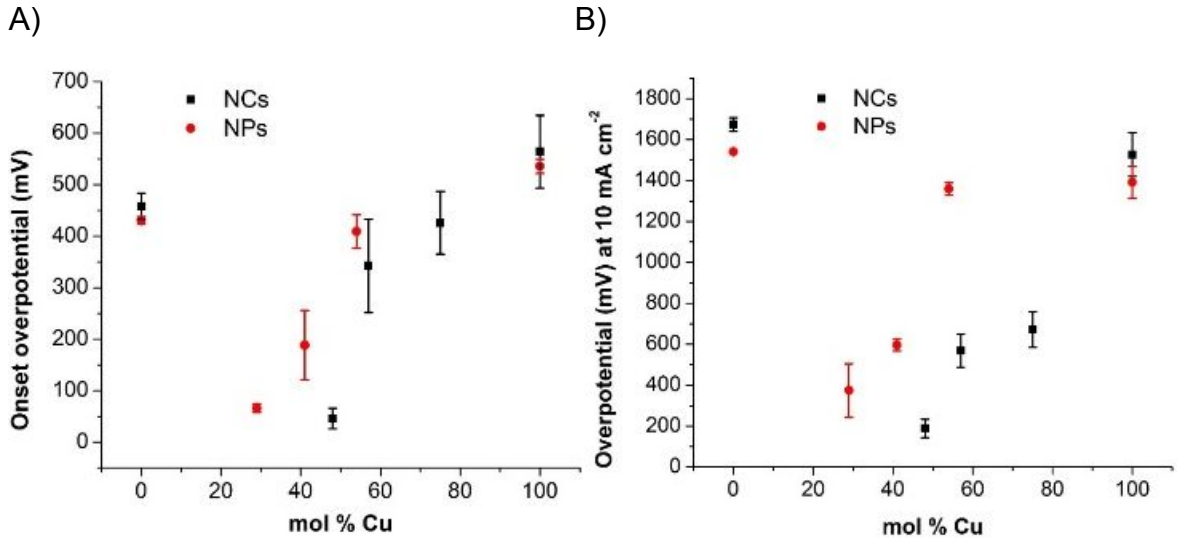

FIGURE 3. Plots of onset overpotentials (A) and overpotentials at 10 mA cm^{-2} (B) for the oxygen evolution reaction in 1 M NaOH using various compositions of Ni-Cu bimetallic nanoclusters (NCs, black) or nanoparticles (NPs, red) on a glassy carbon working electrode.

The onset overpotentials of the Ni-Cu electrocatalysts also depend strongly on the ratio of Ni and Cu present. The lowest overpotentials obtained for both the nanoparticles and nanoclusters is about 50 mV (Figure 3A). This result suggests that the intrinsic surface chemistry that enables catalysis for the nanoparticles and nanoclusters is similar, although the optimal molar composition to achieve this surface chemistry differs when the catalyst size changes. We also evaluated the overpotentials of the nanoparticles and nanoclusters at a current density of 10 mA cm^{-2} because the overpotential at this current density is the primary figure of merit for a practical water-splitting

device.[22] Among the Ni-Cu nanoparticles, the particles with 71:29 mol % Ni-Cu possess the lowest overpotential of ~350 mV at 10 mA cm^{-2}. However, the nanoclusters with 52:48 mol % Ni-Cu exhibit the lowest overpotential of only ~150 mV at 10 mA cm^{-2}, 200 mV less than that of the nanoparticles and among the lowest reported for any OER electrocatalyst (Table S2). Although the nanoparticles and nanoclusters with the lowest overpotentials at 10 mA cm^{-2} have two different molar ratios, the optimal nanoclusters possess a lower overpotential than the nanoparticles. The enhanced activity of the Ni-Cu nanostructured catalysts can be attributed to synergistic effects between Ni and Cu, resulting from differences in bimetallic surface reactivity towards oxygen radical intermediates.[7] For other Ni-Cu materials, it has been demonstrated that oxygen in the form of O_2^{2-}/O^- on the catalyst surface are strongly electrophilic reactants that are very active towards oxidation. These oxygen species are coordinatively unsaturated oxygen complexes that enhance catalyst activity.[23-25] These species also contribute to an increased number of oxygen defects on the catalyst, which act as charge traps and adsorption sites that facilitate charge transfer.[26]

In addition to determining reaction overpotentials, we also evaluated the Tafel slopes of the catalysts from the OER LSVs (Figure S12, ESI). The Ni nanoclusters and nanoparticles possess Tafel slopes near 120 mV dec^{-1}, a value indicative of a rate-limiting single electron transfer step as has been reported for other OER catalysts based on Ni and Ni-Fe.[5] For most of the bimetallic Ni-Cu catalysts, however, the Tafel slopes are much greater than 120 mV dec^{-1}. Large Tafel slopes like these observed with previous OER catalysts typically are indicative of impeded electron transfer kinetics due to surface passivation. The exact origin of surface passivation in these Ni-Cu catalysts is unknown, but given that these large Tafel slope values are not seen in the Ni only catalysts, it is possible that surface passivation results from Cu oxide species formed during catalysis.

We also assessed catalyst activity of the nanoclusters and nanoparticles when taking into account the electrochemically active surface area (ECSA) of the catalysts. The ECSAs of the catalysts were calculated using Pb underpotential (Figure S13, ESI), which is widely used to measure the ECSAs of Cu and Ni systems.[27-29] Because of their smaller diameters, the nanoclusters were found to have ECSAs ~250 times greater than the nanoparticles. When the currents of the OER LSVs of the catalysts are normalized using the ECSAs, the current densities of the nanoclusters are ~10 times less than that of the nanoparticles (Figure S14, ESI). The decreased intrinsic activity of the nanoclusters, at least in terms of reaction kinetics, could be caused by impeded mass transfer arising from the tightly packed layer of capping glutathione ligands that stabilizes nanocluster formation. Nonetheless, the nanoclusters still exhibit lower reaction overpotentials and enhanced geometric current densities as compared to the nanoparticles as discussed earlier.

In addition to catalyst activity, catalyst stability is an important consideration when developing OER electrocatalysts. To assess stability, a series of chronopotentiometry tests of the nanoclusters with the highest OER activity (52:48 mole % Ni-Cu) were performed at a current density of 10 mA cm^{-2} for 1 hour in 1 M NaOH (Figure 4). We first tested the nanoclusters on a typical carbon support (Vulcan XC-72) on a glassy carbon electrode. In this case, the voltage increased quickly and reached 3 V vs. RHE in less than 6 minutes (blue line), indicating that the nanoclusters are highly unstable under these conditions. The instability of the nanoclusters is also demonstrated by cyclic voltammetry (Figure S15, ESI), which shows that the catalytic current density decreases significantly during multiple cycles. To enhance the stability of the nanoclusters, we turned to TiO_2 nanoparticles on carbon paper as an electrode support. Control experiments with bare carbon paper (black line) and TiO_2 nanoparticles on bare carbon paper (red line) show

excellent stability over 1 hour, requiring a voltage of 2.6 and 2.4 V vs. RHE for bare carbon and TiO_2 on bare carbon, respectively. When the nanoclusters are supported by TiO_2 on carbon, the voltage decreased to 1.6 V vs. RHE (green line) and increased much less than without TiO_2 (blue line) over the course of 1 hour. Gas chromatography experiments indicate that the Faradaic efficiency for O_2 production by these Ni-Cu nanoclusters on TiO_2 is 95%. SEM-EDX images of the nanoclusters supported on TiO_2 reveal that the ~20 nm diameter TiO_2 particles were successfully deposited on the carbon paper electrode (Figure S16, ESI). We attribute the enhanced stability of the nanoclusters on TiO_2 to the bonding that occurs between the oxygen in TiO_2 and the carboxylate groups in the glutathione-capped nanoclusters. Analogous TiO_2-carboxylate interactions are widely used in dye-sensitized solar cells and other electrode architectures to enhance device stability.[30-32] The bonding of the nanoclusters to the TiO_2 nanoparticles likely enhances stability by preventing nanocluster aggregation and subsequent catalyst inhibition. Future work will explore other conjugate chemistries that could improve the covalent tethering of the nanocluster catalysts to electrode surfaces with the goal of further increasing the stability of these catalysts.

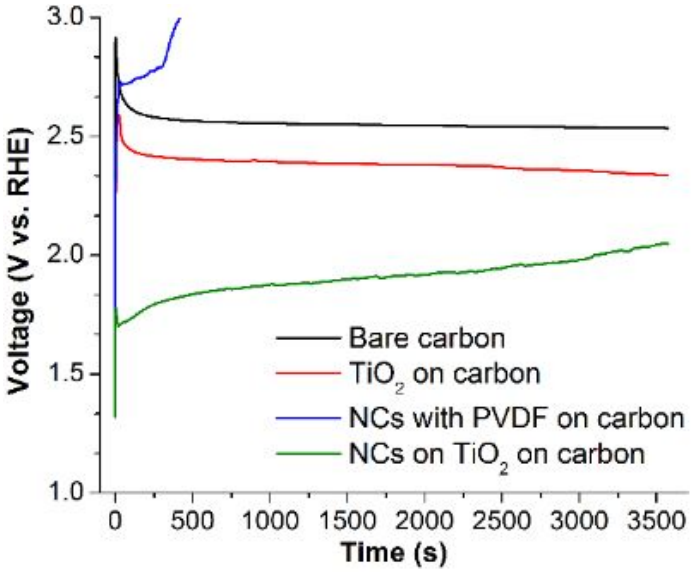

FIGURE 4. Chronopotentiometry curves of carbon (black line), TiO_2 nanoparticles on carbon (red line), Ni-Cu nanoclusters with PVDF on carbon (blue line), and Ni-Cu nanoclusters on TiO_2 nanoparticles on carbon (green line) electrodes at a current density of 10 mA cm^{-2} in 1 M NaOH.

Although the improved catalytic stability of the nanoclusters when anchored to TiO_2 suggests that one degradation mechanism of the catalysts is their detachment from the electrode, electrochemical corrosion of the metals and/or ligand scaffold could also be operative. To evaluate these possibilities, we first conducted MALDI-TOF MS of the 52:48 mol % Ni-Cu nanoclusters after catalysis (Figure S17, ESI). The peak positions in the mass spectra before and after catalysis are similar, indicating that intact glutathione-nanocluster complexes still exist after catalysis. We also performed XRD analysis of the Ni-Cu nanoclusters as-deposited on carbon paper and after ten OER voltammetry cycles (Figure 5). Before catalysis, the XRD spectrum contains peaks ascribable to Ni, Cu, carbon, and polytetrafluoroethylene (PTFE), the last of which is present on the commercially-obtained carbon paper.[15] After catalysis, in addition to the metallic Ni and Cu peaks, additional peaks arising from NiOOH and Cu_2O appear in the spectrum. These results, coupled with the previously discussed voltammetry of the $Ni(OH)_2$/NiOOH redox couple (Figure S8), suggest that the active form of the catalyst consists, at least partially, of NiOOH and Cu_2O.

The Cu Pourbaix diagram indicates that Cu_2O and CuO_2^{2-} are the thermodynamically preferred Cu species under the conditions of the OER LSVs.[33] It is therefore possible that in addition to Cu_2O formation, soluble CuO_2^{2-} is leached from the electrolyte after prolonged catalysis.

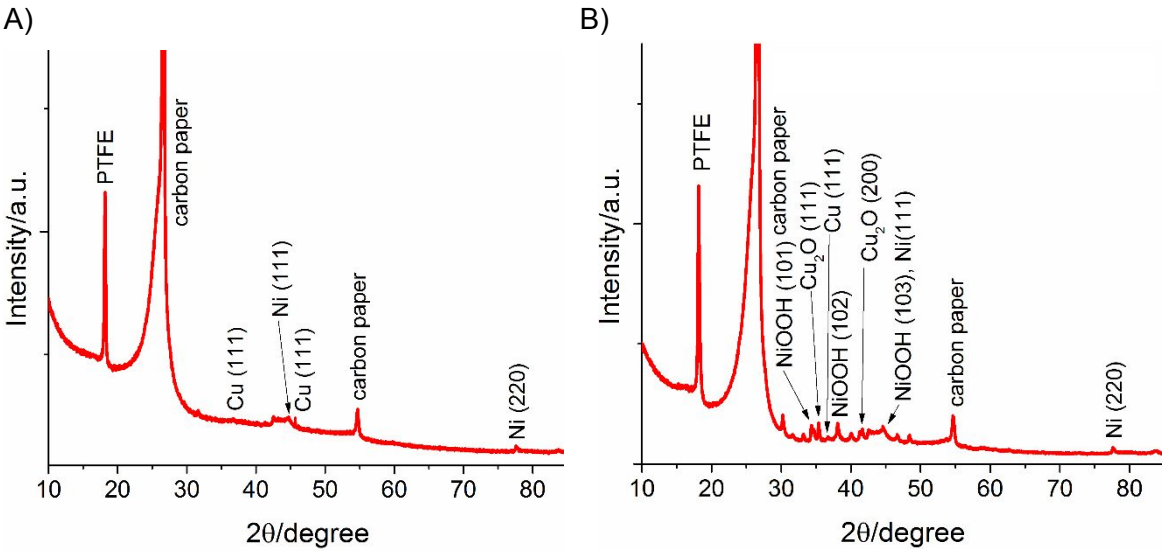

FIGURE 5: XRD spectra of the 52:48 mol % Ni-Cu nanoclusters before (A) and after (B) OER catalysis.

Although the MS and XRD results reveal important structural details of the Ni-Cu nanoclusters, the data do not give information about the structure of the glutathione ligand network, which could dictate catalytic activity. To investigate ligand structure, the FTIR spectra of the nanoclusters were collected in the amide I region. The amide I region (1600-1700 cm^{-1}) of IR spectra are routinely used to determine peptide secondary structures in solution.[34-36] The IR spectrum of the glutathione-nanocluster complex in solution before catalysis (Figure 6, blue) has three distinct peaks at 1620 cm^{-1}, 1636 cm^{-1}, and 1673 cm^{-1}. The peak at 1636 cm^{-1} is assigned to the formation of beta-sheets in small peptides as has been observed previously.[37] Furthermore, a sharp, narrow, intense peak at ~1680 cm^{-1} and a second weaker band at lower frequency are characteristic of peptide aggregation.[38-40] These findings suggest that the as-synthesized nanoclusters contain a well-packed ligand network. In contrast, the IR spectrum of the nanoclusters

after catalysis does not show the signature aggregation band at 1673 cm^{-1} (Figure 6, gray). Instead, the major spectral feature, a distinct band at 1641 cm^{-1} is indicative of a random coil structure. Because the catalyst degrades, these results suggest that the catalysts facilitate the OER at a lower overpotential with a well-ordered ligand network. As a control experiment, the IR spectrum of glutathione by itself was measured (Figure 6, orange). The spectrum has similar spectral features to the complex after catalysis, indicating that the ligand structure of the nanoclusters depends upon catalyst activity. Taken together, from IR analysis and the TiO_2 experiments, we conclude that nanocluster degradation on carbon electrodes occurs both because the catalysts detach from the electrodes and because of changes in ligand structure. Despite these degradation pathways however, the nanoclusters remain largely intact after catalysis as is evidenced by the similarity of the mass spectra before and after catalysis.

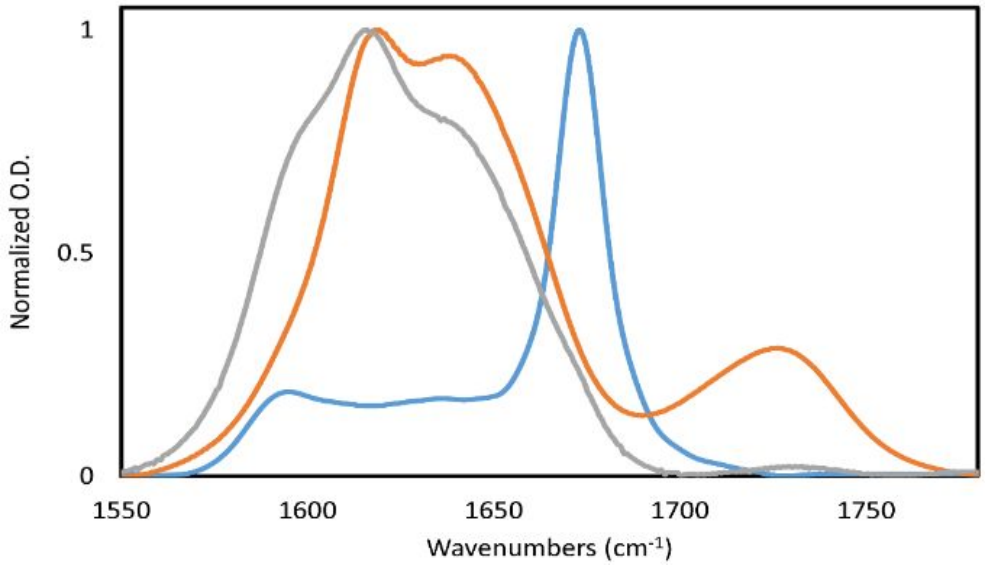

FIGURE 6. Normalized FTIR spectra of the 52:48 mole % Ni-Cu nanoclusters before (blue) and after (gray) catalysis along with the spectrum of glutathione (orange).

Conclusions

In conclusion, we synthesized various compositions of metallic and bimetallic Ni-Cu nanostructured electrocatalysts for the OER. MALDI-TOF MS, high resolution ESI-MS, ICP-MS, XRD, FTIR, and SEM-EDX measurements confirmed the size, molar ratio, and morphology of the nanoclusters and nanoparticles. An optimal molar ratio of Ni-Cu bimetallic nanoclusters (52:48 mol % Ni-Cu NCs) possess an overpotential of ~150 mV at 10 mA cm^{-2}, making it one of the most efficient nonprecious metal OER catalysts reported. The durability of the nanoclusters for OER catalysis can be improved by tethering them via glutathione ligands to an electrode modified with TiO_2 nanoparticles. The promising performance of the Ni-Cu nanoclusters with controllable size and composition opens up future research on this new class of OER electrocatalysts.

Author Information

Corresponding Author
*E-mail: cbarile@unr.edu
Notes

The authors declare no competing financial interest.

Acknowledgements

The authors acknowledge the MacKay Microbeam Lab at the University of Nevada, Reno (UNR) for SEM-EDX analysis and the Shared Instrumentation Laboratory in the Department of Chemistry at UNR for mass spectrometry analysis. The support of the National Science Foundation (CHE-1429768) for the purchase of the powder X-ray diffractometer is gratefully acknowledged. CJB acknowledges the donors of The American Chemical Society Petroleum

Research fund for partial support of this research and Research and Innovation at the University of Nevada, Reno. MJT acknowledges a National Institutes of Health grant (R15GM1224597).

Notes and references

1. H. Zhou, F. Yu, J. Sun, R.He, S. Chen, C.Chu, Z. Ren, *P. Natl. Acad. Sci.* USA 2017, **114**, 5607-5611.

2. B. Oiu, L. Cai, Y.Wang, Z.Lin, Y. Zou, M.Wang, Y,Chai, *Adv. Func. Mater.* 2018, **28**, 1706008-1706018.

3. Q. Shi, C. Zhu, D. Du, Y. Lin, *Chem. Soc. Rev.,* 2019, **48**, 3181-3192.

4. M. Jamesh, X. Sun, *J. Power Sources,* 2018, **400**, 31-68.

5. N. Suen, Hung, S. Hung, Quan, Q. Quan, N. Zhang, Y.Xu, H. M. Chen, *Chem. Soc. Rev.,* 2017, **46**, 337-365.

6. A. Antar, Y. Naimi, D. Takky, IOP Conference Series: Earth and Environmental Science 2018, **161**, 012027.

7. S. Fu, C. Zhu, J. Song, M. H. Engelhard, X. Li, D. Du, Y. Lin, *ACS Energy Lett.,* 2016, **1**, 792-796.

8. Y. Cheng, S. He, J. Veder, R. De Marco, S. Yang, S. Ping Jiang, *ChemElectroChem*., 2019, ***6,*** 3478-3487.

9. J. Nai, H. Yin, T. You, L. Zheng, J. Zhang, P. Wang, Z. Jin, Y. Tian, J. Liu, Z. Tang, L. Guo, *Adv. Energy Mater.* , 2015, **5**, 1401880-1401884.

10. C. Zhu, D. Wen, S. Leubner, M. Oschatz, W. Liu, M. Holzschuh, F. Simon, S. Kaskel, A. Eychmüller, *Chem. Commun.*, 2015, **51**, 7851-7854.

11. Y. T. Lee, R. P. Gautam, S. M. Islam, C. J. Barile, *J. Phys. Chem. C,* 2019, **123**, 1287-1292.

12. M. P. Browne, S. Stafford, M. O'Brien, H. Nolan, N. C. Berner, G. S. Duesberg, P. E. Colavita, M. E. G. Lyons, *J. Mater. Chem. A* 2016, **4** 11397-11407.

13. L. Argueta-Figueroa, T. A. Morales-Luckie, R. J. Scougall-Vilchis, O. F. Olea-Mejia, *Prog. Nat. Sci. Mater.* 2014, ***24*****,** 321-328.

14. X. Gao, Y. Lu, M. Liu, S. He, W. Chen, *J. Mater. Chem. C* 2015, **3**, 4050-4056.

15. H. Pan, C. J. Barile, *J. Mater. Chem. A* 2020, **8**, 1741-1748.

16. C. E. D. Chidsey, *Science* 1991, **251**, 919-922.

17. C. Y. Huang, Z. Getahun, Y. Zhu, J. W. Klemke, W. F. DeGrade, F. Gai, *Proc. Natl. Acad. Sci.* 2002, **99**, 2788-2793.

18. N. Wang, L. Ga, M. Jia, J. Ai, *J. Nanomater.* 2019, **2019**, 1-5.

19. K. Basu, S. Paul, R. Jana, A. Datta, A. Banerjee, *ACS Sus. Chem. Eng.* 2019, **7**, 1998-2007.

20. Y. Li, L. Feng, W. Yan, I. Hussain, L. Su, B. Tan, *Nanoscale* 2019, **11**, 1286-1294.

21. T. T. H. Hoang, A. A. Gewirth, *ACS Catal.* 2016, **6**, 1159-1164.

22. C.C. L. McCrory, S. Jung, J.C. Peters, T. F. Jaramillo, *J. Am. Chem. Soc.* 2013, **135**, 16977-16987.

23. L. Wang, X. Ge, Y. Li, J. Liu, L. Huang, L. Feng, Y. Wang, *J. Mater. Chem. A* 2017, **5**, 4331-4334.

24. J. Fan, Z. Chen, H. Shi, G. Zhao, *Chem. Commun.* 2016, **52**, 4290-4293.

25. Y. Wang, J. Ren, Y. Wang, F. Zhang, X. Liu, Y. Guo, G. Lu, *J. Phys. Chem. C* 2008, **112**, 15293-15298.

26. J. Bao, X. D. Zhang, B. Fan, J. J. Zhang, M. Zhou, W. L. Yang, X. Hu, H. Wang, B. C. Pan, Y. Xie, *Angew. Chem. Int. Ed.* 2015, **54**, 7399-7404.

27. G. Y. Wu, S. E. Bae, A. A. Gewirth, J. Gray, X. D. Zhu, T. P. Moffat, W. Schwarzacher, *Surf. Sci.,* 2007, **601**, 1886-1891.

28. M. Seo, K. Fushimi, H. Habazaki, T. Nakayama, *Corros. Sci.*, 2008, **50**, 3139-3146.

29. Y. Song, R. Peng, D. K. Hensley, P. V. Bonnesen, L. Liang, Z. Wu, H. M. Meyer, M. Chi, C. Ma, B. G. Sumpter, A. J. Rondinone, *ChemistrySelect* 2016, **1**, 6055-6061.

30. W. Chen, S. Nachimuthu, J. Jiang, *Sci. Reports* 2017, **7**, 4979-4991.

31. L. Zhang, J. M. Cole, *ACS Appl. Mater. Inter.*, 2015, **7**, 3427-3455.

32. M. Pastore, T. Etienne, F. De Angelis, *J. Mater. Chem. C* 2016, **4**, 4346-4373.

33. Y. Oh, G. Park, C. Chung, *J. Electrochem. Soc.* 2006, **153**, G617-G621.

34. L. P. DeFlores, Z. Ganim, R. A. Nicodemus, A. Tokmakoff, *J. Am. Chem. Soc.* 2009, **131**, 3385-3391.

35. A. Barth, C. Zscherp, *Q. Rev. Biophys.* 2002, **35**, 369-430.

36. P. Hamm, M. Lim, R. M. Hochstrasser, *J. Phys. Chem. B* 1998, **102**, 6123-6138.

37. C. M. Davis, R.B. Dyer, *J. Am. Chem. Soc.*, 2016, **138**, 1456-1464.

38. Z. Ganim, H.S. Chung, A. W. Smith, L.P. DeFlores, K. C. Jones, A. Tokmakoff, *Acc. Chem. Res.*, 2008, **41**, 432-441.

39. V. Koppaka, P. H. Axelsen, *Biochemistry* 2000, **39**, 10011-10016.

40. S.D. Moran, M.T. Zanni, *J. Phys. Chem. Lett.*, 2014, **5**, 1984-1993.

Table of Contents Entry

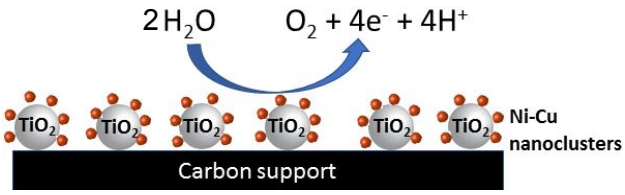

Ni-Cu nanoclusters and nanoparticles form a highly active family of electrocatalysts for the oxygen evolution reaction.